Journal of Computational Physics **170,** 893–916 (2001)
doi:10.1006/jcph.2001.6773, available online at http://www.idealibrary.com on IDEAL®

Approximation and Reconstruction of the Electrostatic Field in Wire–Plate Precipitators by a Low-Order Model

F. Beux,* A. Iollo,† M. V. Salvetti,‡ and A. Soldati§

*Scuola Normale Superiore di Pisa, Pisa, Italy; †Dipartimento di Ingegneria Aeronautica e Spaziale, Politecnico di Torino, Torino, Italy; ‡Dipartimento di Ingegneria Aerospaziale, Università di Pisa, Pisa, Italy; and §Dipartimento di Scienze e Tecnologie Chimiche, Università di Udine, Udine, Italy
E-mail: fbeux@degun.sns.it

Received April 10, 2000; revised January 8, 2001

The numerical computation of the ionic space charge and electric field produced by corona discharge in a wire–plate electrostatic precipitator (ESP) is considered. The electrostatic problem is defined by a reduced set of the Maxwell equations. Since self-consistent conditions at the wire and at the plate cannot be specified a priori, a time-consuming iterative numerical procedure is required. The efficiency of all numerical solvers of the reduced Maxwell equations depends in particular on the accuracy of the initial guess solution. The objectives of this work are two: first, we propose a semianalytical technique based on the Karhunen–Loève (KL) decomposition of the current density field J, which can significantly improve the performance of a numerical solver; second, we devise a procedure to reconstruct the complete electric field from a given J. The approximate solution of the current density field is based on the derivation of an analytical approximation $\tilde{J}$, which, added to a linear combination of few KL basis functions, constitutes an accurate approximation of J. In the first place, this result is useful for optimization procedures of the current density field, which involve the computation of many different configurations. Second, we show that from the current density field we can obtain an accurate estimate for the complete electrostatic field which can be used to speed up the convergence of the iterative procedure of standard numerical solvers.

Key Words: wire–plate precipitators; reduced Maxwell equations; Karhunen–Loève decomposition; low-order model; efficient computations.

1. INTRODUCTION

Electrostatic precipitators (ESPs) are widely used to separate dust particles or aerosols from a carrier fluid. Specifically, dust particles are charged and are then driven toward

0021-9991/01 $35.00

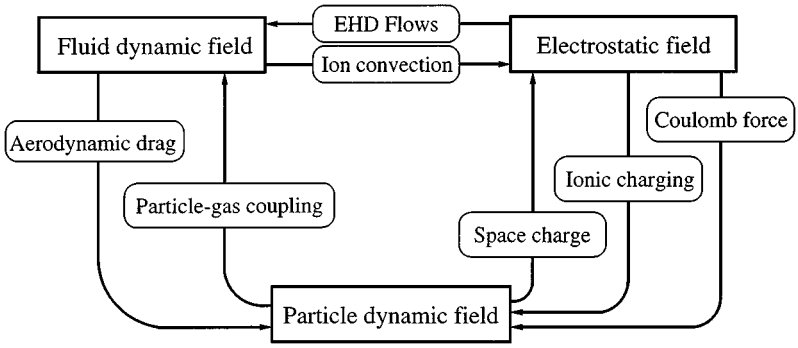

FIG. 1. Coupling among electrostatic field, fluid dynamics, and particle dispersion.

collecting electrodes by an applied electrostatic field. In the widely used wire–plate configuration, the dust-laden gas flows through a rectangular channel bounded by grounded vertical collecting plates. Thin vertical wires are placed in the middle of the channel and are maintained at a potential larger than the local electrical breakdown, to emit ions by corona discharge. The presence of ions is required to charge the dust particles dispersed in the carrier fluid, which are initially neutral. However, the ions also interact with the fluid molecules, which thus acquire momentum so that flows driven by the applied electrostatic field are generated. These flows are called electrohydrodynamic (EHD) flows and couple the fluid mechanics problem with the electric field–space charge problem. A further coupling is introduced by the presence of particles, which, being charged, are coupled with the electrostatic field and are also coupled with the fluid via the aerodynamic drag [1] as shown in Fig. 1. To compute the whole problem, one should solve the reduced Maxwell equations for the electrostatic field and space charge coupled with both particle dynamics and Navier–Stokes equations.

The solution of these equations for one set of parameters appears complex. If an optimal configuration is sought, the task of analyzing accurately the influence of the different parameters on a large number of cases is beyond the capabilities of present-day computers. In the past, we examined specific configurations for ESPs, and we observed the influence of the electrostatic field on particle collection efficiency [2]. Furthermore, we observed also that the large-scale structures generated by electrostatic forces modify the turbulence behavior, in particular near the wall, and for certain configurations this might lead to a significant drag reduction [3]. Based on our previous findings and inspired by the work in [4], tentative innovative configurations for drag-optimized ESPs have been investigated [5] through a direct numerical simulation of the turbulent flow field coupled to the electrostatic field solved by a standard numerical technique. However, since a complete numerical solution of the fluid-dynamic problem coupled with the electrostatic problem is not feasible in an optimization procedure, because of the prohibitive computational requirements, we concluded that more efficient algorithms and/or reduced-order models must be set up for both the electrostatic and the fluid-dynamic problems. Our final goal is to devise a global numerical strategy for ESP optimization and/or control. In this work, we address the electrostatic part in the absence of couplings with fluid-dynamic field and particle-dynamic field. In particular, we propose a semianalytic approximation of the current density field, which has two important applications. First, it makes it possible to express the electrostatic body force appearing in the fluid-dynamic equations as a function of a reduced number of parameters, which

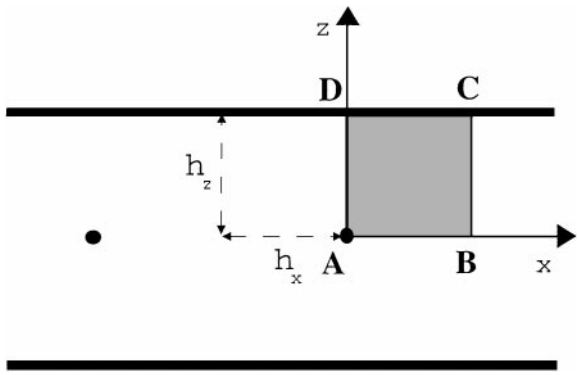

FIG. 2. Wire–duct precipitator geometry and computational domain.

can be easily treated in a global optimization procedure. Second, it leads to more efficient algorithms for the numerical solution of the space-charge coupled problem.

Consider the ideal wire–plate ESP configuration shown in Fig. 2. Under certain conditions, the ion discharge may be assumed to be uniform along the wire, and the electrostatic problem can be solved in two dimensions. A major difficulty in the computation of this problem is that all the conditions at the wire and at the plate cannot be specified a priori in a self-consistent way. The usual procedure is to start from an initial guess of the charge density and electric potential fields, ρ and V, and to iterate the numerical solution of the reduced Maxwell equations, adjusting at each iteration the value of V (as, e.g., in Refs. [6–8]) or ρ (as, e.g., in Refs. [9–11]) at the wire, until convergence is achieved. As a consequence, the numerical computation of the electrostatic field is considerably time-consuming. Several algorithms have been used in the literature to reduce the computational cost and, in particular, by coupling efficient discretization and convergence acceleration techniques (e.g., pseudo-transient approach with relaxation and multigrid [11] or Newton algorithm [12]). A different approach has been proposed in Ref. [13], in which the introduction of an auxiliary equation and an auxiliary variable makes it possible to solve the problem with Newton iterations for all the unknowns simultaneously. However, no explicit information is given in Ref. [13] on the efficiency of this method compared to previous ones.

In all cases, the computational procedures used for the solution of this problem require an initial guess of the potential and charge density fields. Usually (see, for instance, [6, 7, 9]), a free space-charge field is assumed and then an analytical expression for the potential is obtained [14].

In the present paper, we propose a semianalytical procedure, based on the Karhunen–Loève (KL) decomposition [15], to parameterize the current density field, J (Section 3). This allows J to be expressed as a function of very few KL modes. This result is useful in control or optimization procedures in electrostatic precipitators, such as those mentioned previously, in which the electrostatic field must be optimized to reduce turbulent friction drag at the plates or to increase particle collection efficiency. Indeed, the electric volume force exerted on the fluid depends only on the current density field; therefore, following the proposed KL decomposition, optimization procedures may derive the optimal J field acting on a significantly reduced number of parameters. Furthermore, this allows the optimization algorithm to be carried out only for the fluid dynamic part, using J as a control parameter, without solving the reduced Maxwell equations at each step. A procedure described in Section 5 also permits all the operative electrostatic variables from the optimal J field given

by the ESP optimization algorithm to be obtained. The proposed parameterization of the current density field has a second relevant application. Indeed, starting from it, an estimate of the complete electrostatic field is obtained as described in Section 4. It is shown that this estimate, which is computed at a negligible computational cost, is in many cases accurate enough to be an acceptable approximation of the solution. Otherwise, it can be used as an initialization for standard numerical solvers leading to dramatic gain in the efficiency of the numerical algorithm.

2. PROBLEM DESCRIPTION AND ASSESSMENT OF A FINITE-DIFFERENCE SOLVER

We consider a wire–duct electrostatic precipitator configuration, i.e., a series of equally spaced wires at high voltage placed in the midplane between two parallel grounded plates. The electrical phenomenon is characterized by a nonuniform electrostatic field. The space charge is generated by ion emission from the corona around the wire and is also characterized by a nonuniform distribution. Neglecting the magnetic effects and considering the steady state, the governing electrostatic equations can be expressed as

$$\Delta V = -\frac{\rho}{\epsilon_0}, \tag{1}$$

$$\rho^2 = \epsilon_0 \nabla\rho \cdot \nabla V, \tag{2}$$

where ρ is the space-charge density, V is the electrical potential, and ϵ_0 is the permittivity of the gas. The electric field and the current density are obtained from V and ρ as follows: $E = -\nabla V$ and $J = \rho\beta E$, where β is the ionic mobility.

Because of symmetry considerations, the computational domain can be reduced to the rectangle ABCD of dimensions $h_x \times h_z$ as shown in Fig. 2, with Neumann boundary conditions $E_z = 0$ along AB and $E_x = 0$ along BC and DA. To close the previous system of equations, Dirichlet conditions are also applied by setting the potential at the grounded plate to zero, i.e., along CD, and by imposing both potential and charge density at the wire (point A). The input values in our procedure are the average current density at the plate J_p, the wire potential V_0, and the wire radius a. They can be specified from experimental data, if available. In our computations, experimental values are used for V_0 and a, while the value of J_p is calculated using a current–voltage formula defined in [16]. More precisely, the following equation is numerically solved by means of a Newton algorithm,

$$\frac{3J_p}{\beta\epsilon_0}\left(V_0 - V_0^S + \frac{\pi a h_z}{2h_x}E_c\right) = \left[\left(\frac{\pi a}{2h_x}E_c\right)^2 + \frac{2h_z}{\beta\epsilon_0}J_p\right]^{3/2} - \left(\frac{\pi a}{2h_x}E_c\right)^3, \tag{3}$$

where E_c is the strength of the electric field at the corona surface and V_0^S is the corona onset voltage, i.e., V_0 corresponding to $J_p = 0$. The starting voltage can be obtained by the formula $V_0^S = a\ln(d/a)E_c$, where d is an equivalent cylinder radius defined in [17]. E_c is determined by the semiempirical Peek's formula [18] for a gas at standard pressure and temperature and for a polished wire:

$$\tilde{E}_c(a) = \mathcal{D}\left(1 + \frac{\mathcal{E}}{\sqrt{a}}\right). \tag{4}$$

The $\mathcal{D}$ and $\mathcal{E}$ coefficients are taken equal to 32.3×10^5 and 0.02619 in SI units, respectively (see [11]).

The wire-charge density ρ_0 is not known a priori. It is initially estimated as a function of J_p and a using the following wire condition [6]:

$$\rho_0 = \frac{2J_p h_x}{\pi a \beta \tilde{E}_c}. \tag{5}$$

Then, a numerical algorithm, similar to the one proposed in Ref. [9], is applied. The knowledge of ρ_0 and of the initial ρ and V fields makes it possible to solve Eq. (2), and then, using the updated ρ field, Eq. (1) is solved giving a new potential field. The value of ρ_0 is adjusted and the computation of ρ and V fields repeated until the average current density at the plate differs from the desired one J_p within a specified tolerance. More precisely, the convergence criterion is

$$\left|J_p - J_p^d(k)\right| / J_p < c_J, \tag{6}$$

where $J_p^d(k)$ is the average plate density charge computed at iteration k and c_J is the specified tolerance. The adjustment of ρ_0 is directly correlated with the previous convergence criterion as

$$\rho_0(k+1) = \rho(k)\left[1 + \lambda\left(J_p - J_p^d(k)\right)/J_p\right],$$

where λ is a constant given a priori ($\lambda = 0.01$ herein). Note that $\tilde{E}_c$ defined by Eq. (5) is used in the algorithm only to find an initial value of ρ_0. The corona electric field E_c is not an input value of the problem and thus is varied during the computation.

As for the numerical discretization of Eqs. (1) and (2), the finite-difference method (FDM) has often been used, particularly in early studies (e.g., [6, 9]). However, to more accurately compute the near wire region characterized by strong gradients, other approaches have been developed: non-Cartesian FDM [8] and methods which can use unstructured grids, such as the finite-element method (FEM) [10, 13] or the finite-volume method (FVM) [11]. Moreover, FEM, which is well adapted to the solution of the elliptic Poisson equation, can be combined with methods suitable for the hyperbolic equation, e.g., FEM–FDM [7], FEM–FVM [12], FEM, and method of characteristics [19, 20] (for a review see [11]).

The present approach is based on a finite-difference method similar to the one defined in Ref. [6], with a uniform value of β and a nonuniform grid system. This method is certainly not the most efficient one among those proposed in the literature; however, comparisons between experimental and numerical data have shown that accurate solutions can be obtained.

In particular, we consider a wire–duct precipitator configuration that has been studied numerically (e.g., [7]) as well as experimentally [21]. This test case is characterized by $h_z = 0.1143$ m, $h_x = 0.0762$ m, $a = 0.152$ mm, and $V_0 = 25.415$ kV. With ionic mobility of 1.9×10^{-4} m^2/V s, the current–voltage formula (Eq. (3)) gives $J_p = 3.77 \times 10^{-4}$ A/m^2. We will refer to this configuration as configuration $\mathcal{A}$. We used four different uniform grids with 23×34, 34×51, 45×67, and 67×99 points, respectively. A 23×34 nonuniform grid, with points clustered near the wire, has also been used. The sensitivity of the solution to the convergence criterion has been preliminary analyzed, and it has been found that independence is reached when the error between computed and specified J_p is less than 0.1%, i.e., $c_J = 0.001$ in Eq. (6). Thus, all the results presented below are obtained with this convergence tolerance. In Figs. 3a and 3b, the potential distributions obtained with different meshes are compared with the experimental data of [21]. If we exclude the coarsest uniform grid, the results are independent of grid resolution,

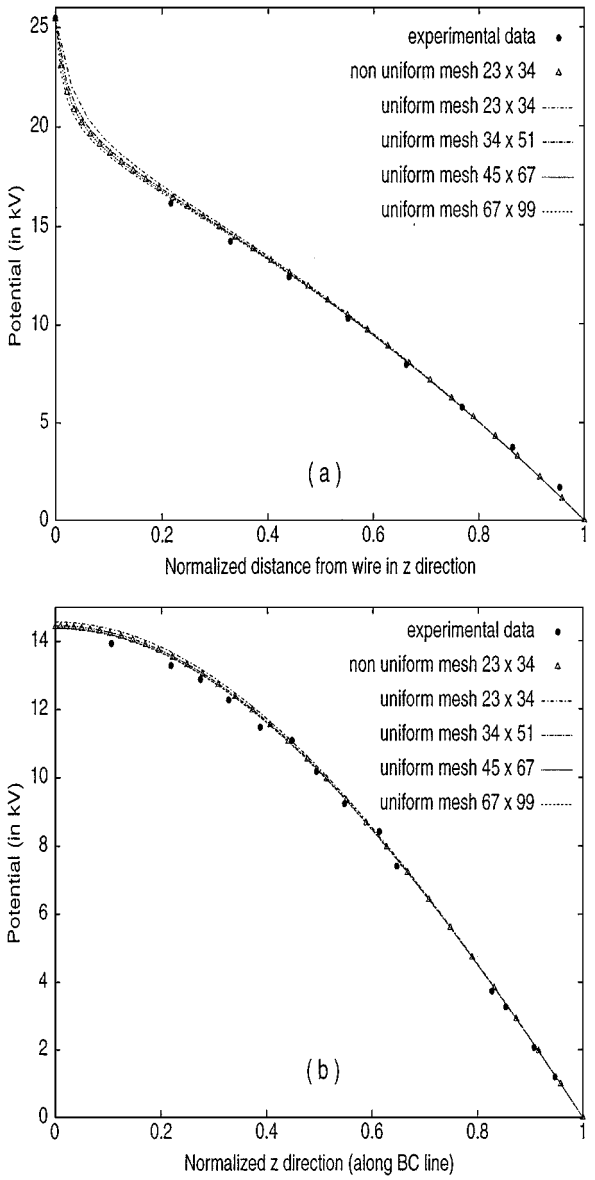

FIG. 3. Comparison between electric potential fields obtained with different meshes and experimental data from [21], for $h_z = 0.1143$ m, $h_x = 0.0762$ m, $a = 0.152$ mm, and $V_0 = 25.415$ kV. (a) Distribution along AD and (b) distribution along BC.

except for slight differences observed near the wire as shown in Fig. 3a, and all are in good agreement with experiments. The same conclusions can be drawn from comparisons carried out for different experimental configurations (not shown here for the sake of brevity). In particular, the use of the 23×34 nonuniform grid allows us to satisfactorily capture the strong gradients near the wire with reduced computational times. Therefore, the electrostatic fields obtained by the finite-difference solver on this nonuniform grid will be considered as reference solutions to evaluate the accuracy of the proposed procedures.

3. PARAMETERIZATION OF THE CURRENT DENSITY FIELD

3.1. *Analytical Approximation*

In this section, the procedure used to obtain an analytical approximation of the current density field is described.

The governing equation for J is

$$\nabla \cdot J = 0, \tag{7}$$

which represents the continuity of steady currents. Boundary conditions for the considered problem are (see Fig. 2) $J_z = 0$ on AB, $J_x = 0$ on BC, CD, and DA, and $J_r = 2J_p h_x/\pi a$ at the wire, where J_r is the radial component of the current density vector. It is clear that Eq. (7) and these boundary conditions are not sufficient to uniquely determine J.

We wish to obtain here an approximation, $\tilde{J}$, of the exact current density field, which satisfies Eq. (7) and the boundary conditions mentioned above. To derive an analytical expression of $\tilde{J}$, the following assumption is made:

$$\nabla \times \tilde{J} = 0. \tag{8}$$

By writing $\tilde{J}$ as $\beta\tilde{\rho}\tilde{E}$, it can easily be shown that hypothesis (8) is equivalent to assuming the electric field and the charge density gradient to be parallel. In particular, this implies that a function Φ exists such that $\tilde{J} = \nabla\Phi$. Using Eq. (7), Φ can be determined from

$$\nabla^2\Phi = 0 \tag{9}$$

with the Neumann boundary conditions derived from those for J. This problem has now a unique solution that can be obtained from classical tools used in hydrodynamic problems, such as singularity distributions and elliptic functions. In particular, using the reflection technique, it can be shown that Eq. (9) and the corresponding boundary conditions are satisfied by an infinite sequence in the x direction of sources of intensity $4J_p h_x$ located at $(\pm 2kh_x, 0)$, $k = 1, \ldots, \infty$, and by an infinite row of alternating sources and sinks of intensity $4J_p h_x$ along z at $(0, \pm 2jh_z)$, $j = 0, \ldots, \infty$ (j even corresponds to a source, while j odd to a sink). Finally, $\tilde{J}_x$ and $\tilde{J}_z$ can be obtained as the real and the imaginary part of the complex function

$$\Psi(x, z) = 4J_p h_x \left[\zeta(x + iz) - \zeta(x + iz - 2h_z)\right], \tag{10}$$

where ζ denotes the Weierstrass ζ function (see, for instance, [22]) and $i = \sqrt{-1}$.

Since, in general, assumption (8) is not verified by the exact solution of Eqs. (1) and (2), $\tilde{J}$ obtained in this way can be considered only an approximation of the exact current density field. It can be easily verified, however, that $\tilde{J}$ satisfies the boundary conditions of the original nonlinear problem. In particular we have

$$\frac{1}{2h_x}\int_{-h_x}^{h_x} J_z(x, h_z)\, dx = J_p. \tag{11}$$

In Figs. 4a and 4b, the isocontours of the approximate and FD (i.e., obtained from the standard finite-difference solver) J_z are plotted for configuration $\mathcal{A}$. Note that J_z is characterized by high values in a small region near the wire, which corresponds to the white

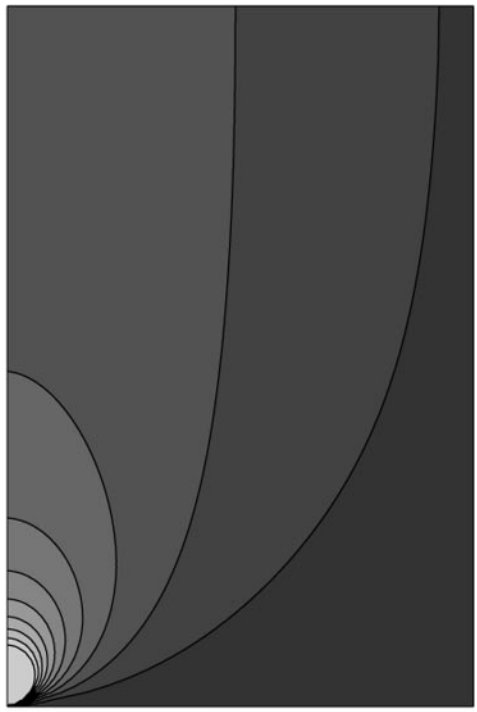

(a)

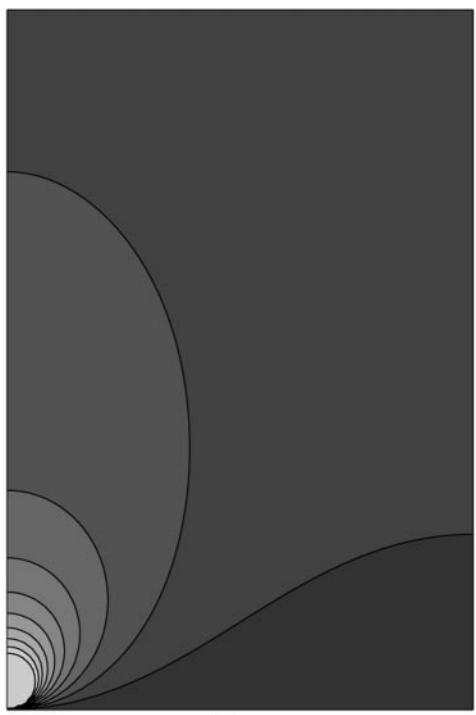

(b)

FIG. 4. Isocontours of (a) J_z and (b) $\tilde{J}_z$. Isocontours range from 0 (black) to 0.002 A/m^2 (white) with a step of 2×10^{-4}.

zone in the figures and is well captured by the analytical approximation. The maximum value in the field is about 0.12 A/m^2 at the wire. In Fig. 4 only isocontours ranging from 0 to 0.002 A/m^2 are shown, to compare very small variations (of 2×10^{-4} A/m^2), in particular, near the plate.

In spite of the differences visible between Figs. 4a and 4b, the global behavior of the analytic field is rather close to the reference FD one. The same considerations can be made for the component J_x (not shown here for the sake of brevity). Thus, a function $\mathcal{J} = J - \tilde{J}$ which satisfies Eq. (7) can be defined, but with homogeneous boundary conditions; this field can be easily decomposed by using the KL technique as shown in Section 3.2.

Moreover, as shown in Figs. 4a and 4b, $\tilde{J}$ is not too far from the reference FD solution, and, thus, it can be used to derive an approximation of the exact electrical field. This can be employed as an initial condition for the numerical solution of the original electrostatic problem (see Section 4).

3.2. *Karhunen–Loève Decomposition*

The KL decomposition, classically used in probability theory [15], has also been utilized in fluid dynamics as a reduced-order model. In that context, it is usually called proper orthogonal decomposition (see, e.g., [23]) and is employed to describe the dynamical behavior of the flow by considering only a finite number of modes.

In the present section, this technique is employed for the parameterization of the deviation of the FD current density field from the approximate one. As mentioned previously, the analytical approximation $\tilde{J}$ satisfies the boundary conditions for the current density field, and, in particular, the average value of $\tilde{J}$ at the plate is equal to J_p. Thus, the Karhunen–Loève decomposition is applied to the remaining homogeneous part of the current density field.

For a fixed configuration of the wire–plate precipitator, i.e., for given h_x and h_z, the current density depends both on space position $X = (x, z)$ and on electric configuration $T = (V_0, a)$ (J_p is obtained from T using a current–voltage formula). Starting from a set of n_s discrete J fields obtained for different T configurations, a Karhunen–Loève decomposition which supplies the current density field as a function of T can be defined. More precisely, from a set of n_s snapshots J_T^l, the KL technique generates n_s modes, $\varphi_j = \sum_l \alpha_{lj}(J_T^l - \tilde{J}_T^l)$, which are mutually orthogonal basis functions, with respect to the canonical inner product in the Hilbert space L^2. These modes have been defined to give an optimal representation of $(J_T^l - \tilde{J}_T^l)$ in the L^2 norm, as explained, for example, in [23]. The coefficients α_{lj} are obtained as the components of the jth eigenvector of the correlation matrix $\mathcal{K}$ ($\mathcal{K}_{lj} = \langle J_T^l - \tilde{J}_T^l, J_T^j - \tilde{J}_T^j \rangle / n_s$). The following decomposition is then obtained for J:

$$J(X, T) = \tilde{J}(X, J_p(T)) + \sum_{j=1}^{n_s} c_j(T)\varphi_j(X) \quad \text{where } c_j = \langle J - \tilde{J}, \varphi_j \rangle. \tag{12}$$

The reconstructed J depends on the snapshots chosen for the decomposition and, also, on n_m, the number of modes used for the reconstruction:

$$J^R(x, z) = \tilde{J}(x, z) + \sum_{j=1}^{n_m} c_j \varphi_j(x, z) \quad \text{with } n_m \leq n_s. \tag{13}$$

The following discrete approximation is used for the computation of the inner products involved in the present procedure,

$$u, v \in (L^2(D))^2 : \langle u, v \rangle_d = \sum_{i,k} \mathcal{A}_{i,k} \langle u(x_i, z_k), v(x_i, z_k) \rangle_{\mathbb{R}^2}, \tag{14}$$

where $\mathcal{A}_{i,k}$ is the area of a cell centered on (x_i, z_k) and D is the computational domain.

For the construction of the database of snapshots, the wire–duct precipitator geometry of Fig. 2 is employed. Ten different configurations are defined by varying the wire radius between 0.1 and 1.016 mm, the plate current density between 5×10^{-5} and 1.557×10^{-3} A/m^2, and the ionic mobility between 1.6×10^{-4} and 1.9×10^{-4} m^2/V s. Five configurations coincide with those in the experiments in Ref. [21], whereas the other five are defined by applying the current–voltage formula to specify V_0, a, and J_p consistently. In all cases, J is obtained numerically by using the algorithm presented in Section 2. The nonuniform 23×34 mesh has been used, since it has been shown in Section 2 that an accurate estimate of the electrostatic field is obtained with this grid resolution. Thus, the numerically computed J is here considered the reference FD solution.

As an example of the accuracy of the KL reconstruction, let us consider the reconstructed field obtained with $n_s = 10$ and $n_m = 2$ for the previously defined configuration $\mathcal{A}$.

In Fig. 5a, the z distribution of J_z^R at $x = 0.0234$ m is compared to the FD solution. The same comparison is made in Fig. 5b for the x distribution of J_x^R at $z = 0.0387$ m. The reconstructed field collapses onto the FD one.

To obtain a global indicator of the difference between the FD solution and the reconstructed one, the following error is defined: $e_N = \| J - J^R \|_d / (N J_p)$, where $\| \cdot \|_d$ is the norm associated to the discrete scalar product $\langle \cdot, \cdot \rangle_d$ defined in Eq. (14) and N is the number of mesh points. The normalization by J_p allows different configurations to be compared.

In Fig. 6, e_N is plotted for the same previous configuration as a function of n_m, i.e., the number of KL modes used for the reconstruction (note that $n_m = 0$ simply corresponds to $J^R = \tilde{J}$). The values obtained by using all the 10 J fields ($n_s = 10$) and those computed by considering only 3 of them ($n_s = 3$) are shown. Note that the case analyzed in Fig. 5 corresponds to $e_N = 5.91 \times 10^{-4}$. Thus, in both cases good accuracy is obtained with few KL modes. Surprisingly, the reconstruction accuracy obtained with only 3 snapshots is better than that corresponding to the 10 snapshots. This is because this configuration coincides with one of the snapshots used for the KL basis definition. In general, the lower the number of considered snapshots, the higher the importance of each one in the basis definition, and hence its KL reconstruction is accurate.

Results obtained for the second configuration, which is not among the 10 fields used for the KL basis definition, are also reported in Fig. 6. In this case, good accuracy is obtained only by using all of the 10 snapshots. However, very few modes are again sufficient to obtain an accurate reconstruction of J.

The previous results are only a few examples of many other tests which have been carried out and are not reported here for the sake of brevity. In all the cases considered, it appears, first, that J can be accurately parameterized by very few KL modes (less than 4) and, second, that a reasonable number of snapshots is needed to construct the KL basis.

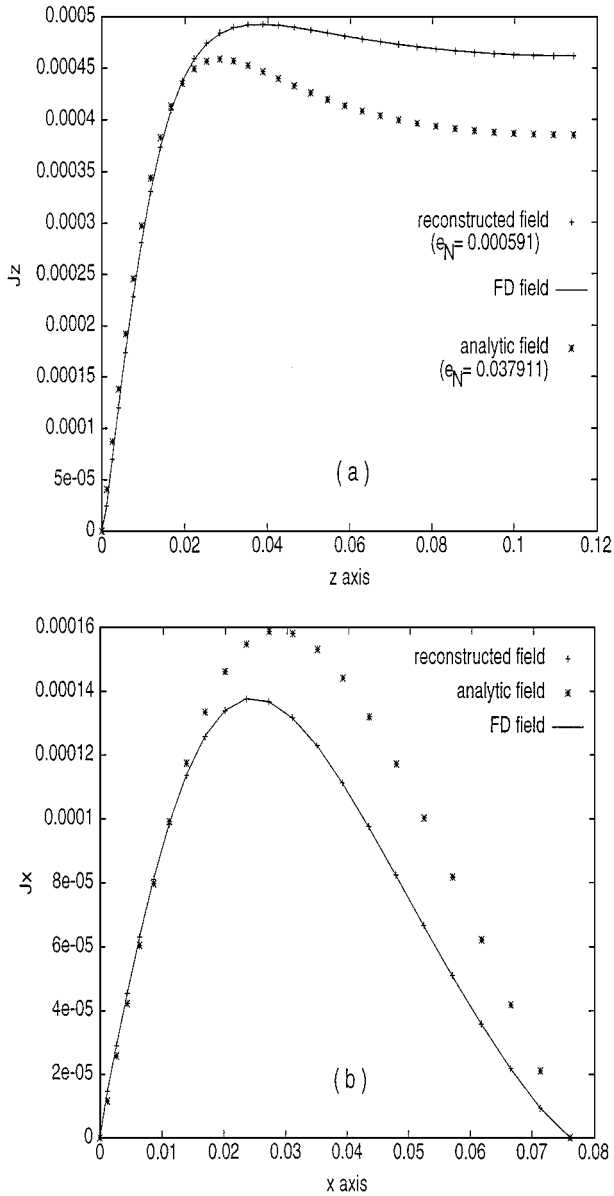

FIG. 5. Comparison of current density fields ($V_0 = 25.415$ kV and $a = 0.152$ mm): reference numerical solution J, analytic approximation $\tilde{J}$, and reconstructed field J^R, with $n_s = 10$ and $n_m = 2$. (a) z component at $x = 0.0234$ m and (b) x component at $z = 0.0387$ m.

4. EFFICIENT COMPUTATIONS BY SUITABLE INITIALIZATION

4.1. *Methodology*

The procedure for the computation of the wire–duct electrostatic precipitator requires an initialization of the charge density and electric potential fields and thus a first a priori estimation of these two fields. Following Cooperman [14], the usual way is to assume the space charge uniformly equal to zero and then to solve a Laplace equation for the potential. However, this initialization gives fields V, ρ, E, and J rather far from the FD solution. A

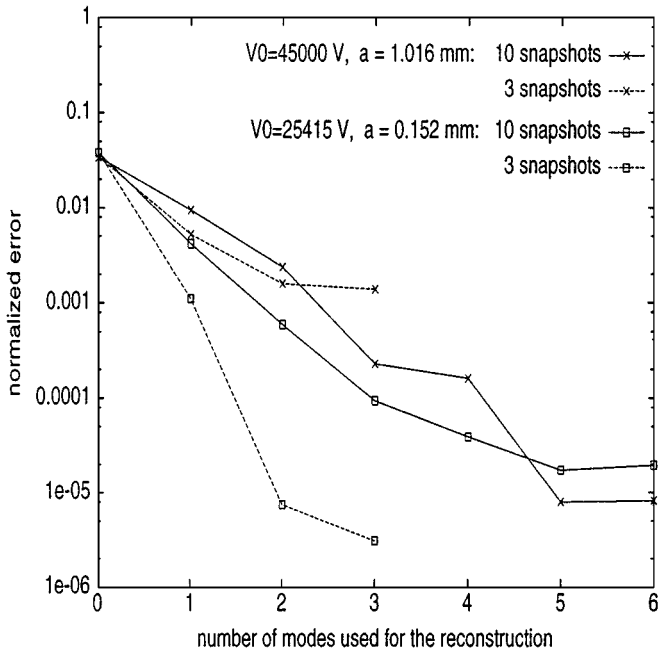

FIG. 6. Normalized error e_N as a function of n_m for $n_s = 10$ and $n_s = 3$ and for two different configurations.

better initial field can be obtained from the previously described analytic approximation and parameterization of J. More precisely, we define potential, electric, and charge density fields using only the knowledge of J_p, a, and V_0. From J_p, an approximate current field $\tilde{J}$ is defined as described in Section 3.1 and a classical estimation of the wire-charge density value, ρ_0, is obtained by Eq. (5). Starting from $\tilde{J}$ and ρ_0 a charge density field can be obtained. Indeed, the following equation in ρ and J can be easily derived from Eq. (2):

$$\frac{\beta}{\epsilon_0}\rho^3 + \nabla\rho J = 0. \tag{15}$$

Equation (15) is simply a modification of the continuity equation for the current density field (Eq. (2)), thus also being a nonlinear hyperbolic equation in ρ. The numerical approximation of this equation can be carried out in a way similar to that for Eq. (2), i.e., by using a finite-difference approach similar to the one defined in Ref. [6]. Finally, the following discretized expression of the charge density field is obtained,

$$\rho_{i,k} = \left[-\frac{\mathcal{B}_{i,k}}{2} + \sqrt{\mathcal{C}_{i,k}}\right]^{1/3} - \left[\frac{\mathcal{B}_{i,k}}{2} + \sqrt{\mathcal{C}_{i,k}}\right]^{1/3}, \tag{16}$$

where

$$\begin{cases} \mathcal{B}_{i,k} = -\frac{\epsilon_0}{\beta}\left[\frac{J_x^{i,k}}{\Delta_x^i}\rho_{i-1,k} + \frac{J_z^{i,k}}{\Delta_z^k}\rho_{i,k-1}\right] & \Delta_z^k = z_k - z_{k-1},\ \Delta_x^i = x_i - x_{i-1}, \\ \mathcal{C}_{i,k} = \left(\frac{\mathcal{A}_{i,k}}{3}\right)^3 + \left(\frac{\mathcal{B}_{i,k}}{2}\right)^2 \quad \text{with } \mathcal{A}_{i,k} = \frac{\epsilon_0}{\beta}\left[\frac{J_x^{i,k}}{\Delta_x^i} + \frac{J_z^{i,k}}{\Delta_z^k}\right]. \end{cases}$$

For a suitable J, and, in particular, if J_x and J_z have only nonnegative values, as in the present case, $\rho_{i,k}$ is well defined by Eq. (16).

For a fixed wire-charge density value ρ_0 and a given J, the entire charge density field is obtained explicitly from Eq. (16), coupled with the following boundary conditions: $\rho_{1,1} = \rho_0$, $J_x^{1,k} = 0$, and $J_z^{i,1} = 0$. From the knowledge of ρ and J, the electric field is immediately derived from $E = J/(\beta\rho)$ and the potential V is obtained from $E = -\nabla V$. The first way to reconstruct V is to use an upwind first-order finite-difference scheme: $V_{i,k-1} = V_{i,k} + \Delta_z^k E_z^{i,k}$. This appears to be a natural way in our formulation because it is exactly the inverse procedure of the one used in the Maxwell solver to obtain E_z from V. Since the potential is equal to zero at the plate, $V_{i,k}$ can be expressed as

$$V_{i,k} = \sum_{s=k+1}^{n_k} \Delta_z^s E_z^{i,s}. \tag{17}$$

One possible drawback to this construction is that only information from the second component of the electric field has been used. Moreover, in this way we have, first an accumulation of approximation errors moving away from the plate, i.e., when k decreases, and second, near the wire–wire middle plane, $\tilde{J}$ gives a poor approximation of the exact current density field. This is clearly shown in Fig. 7, in which the z average of the relative error obtained for configuration $\mathcal{A}$ is plotted. The z-average relative error is defined as

$$e_z^i(\tilde{J}) = \frac{1}{2(n_k - 2)} \sum_{k=2}^{n_k - 1} \left[\frac{\left| J_{i,k}^x - \tilde{J}_{i,k}^x \right|}{J_{i,k}^x} + \frac{\left| J_{i,k}^z - \tilde{J}_{i,k}^z \right|}{J_{i,k}^z} \right].$$

The approximation of the potential field is inaccurate near the line BC, and in particular, close to point B.

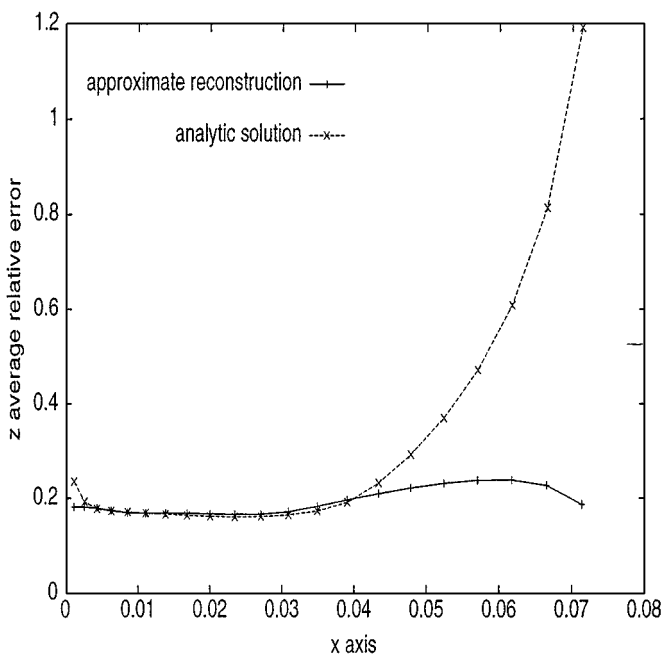

FIG. 7. The z-average relative error e_z^i for both $\tilde{J}$ and J^R (with $i_0 = 3n_i/4$). $V_0 = 25.415$ kV and $a = 0.152$.

As an alternative approach, the E_x field can be used to relate the potential evaluated at two points in the x direction. This is done by integrating with respect to x between x_j and x_i, and using a trapezium formula, the following reconstruction is found:

$$V_{i,k} = V_{j,k} - \frac{1}{2}\sum_{q=j}^{i-1}\left(E_x^{q,k} + E_x^{q+1,k}\right)\Delta_x^{q+1}. \tag{18}$$

However, since in this case the Dirichlet boundary condition is not available for V in the x direction to initialize the procedure, a mixed approach using both E_z and E_x can be envisaged, using the first approach in the left part of the domain and the second one in the right part. More precisely, let i_0 be an index i larger than one; for i smaller than or equal to i_0, Eq. (17) is used, whereas for $i > i_0$ relation (18) is employed with $j = i_0$. This allows, in particular, the Neumann conditions to be verified on the wire–wire middle plane, as shown for instance in Fig. 8.

In summary, an initial field for the numerical solution of the governing equations of the wire–duct precipitator problem has been defined from the analytical field $\tilde{J}$ by using Eqs. (16)–(18). However, in the described procedure, the wire potential V_0 has not been used explicitly. Thus, the obtained initial field may be characterized by a value of V_0 significantly different from the exact one, as shown for instance in Fig. 8. To further improve the accuracy of the initial field evaluation, the same procedure can be repeated using the parameterization of the current density field described in Section 3.2, i.e., starting from a J which verifies Eq. (13). The coefficients c_l cannot be exactly computed as in Eq. (12) because the exact field is not known a priori; thus they are obtained here by an optimization algorithm to obtain a wire-potential value close to V_0. More precisely, the KL coefficients are computed

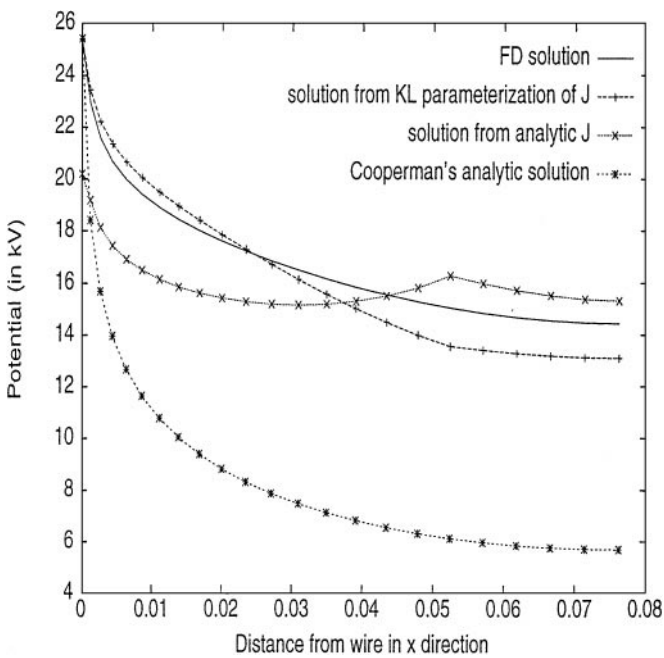

FIG. 8. Potential along AB ($a = 0.152$ mm and $V_0 = 25.415$ kV) for the fully converged solution, Cooperman's analytic solution, the solution from $\tilde{J}$, and the solution from J^R with $n_s = 10, n_m = 6$, and $i_0 = 3n_i/4$.

by minimizing the functional $I = (V_{1,1} - V_0)^2/2V_0^2$. Thus, starting with all the coefficients equal to zero, i.e., J^0 equal to $\tilde{J}$, the following iterative procedure is carried out:

- Charge density and potential fields are obtained using Eq. (16) and Eqs. (17) and (18), respectively.
- The mode coefficients are updated using a gradient descent method:

$$l = 1, \ldots, n_m \quad c_l^{p+1} = c_l^p - \omega \frac{\partial I^p}{\partial c_l}.$$

Using the expression of $V_{1,1}$, i.e., $V_{1,1} = \sum_{k=2}^{n_k} \Delta_z^k E_z^{1,k}$, and introducing the J field and its parameterization, the derivatives of I can be written as

$$\frac{\partial I}{\partial c_l} = \frac{(V_{1,1} - V_0)}{\beta V_0^2} \sum_{k=2}^{n_k} \frac{\Delta_z^k}{\rho_{1,k}} \left[(\varphi_z)_l^{1,k} - \frac{1}{\rho_{1,k}} \left(\tilde{J}_z^{1,k} + \sum_{j=1}^{n_m} c_j (\varphi_z)_j^{1,k} \right) \frac{\partial \rho_{1,k}}{\partial c_l} \right], \quad (19)$$

where $\frac{\partial \rho_{1,k}}{\partial c_l}$ can be expressed exactly from Eq. (16) as a function of $\frac{\partial \rho_{1,k-1}}{\partial c_l}$ in the following way,

$$\begin{aligned} \frac{\partial \rho_{1,k}}{\partial c_l} = {} & \frac{1}{6} \left[-\frac{\mathcal{B}_{1,k}}{2} + \sqrt{\mathcal{C}_{1,k}} \right]^{-2/3} \left[-\frac{\partial \mathcal{B}_{1,k}}{\partial c_l} + [\mathcal{C}_{1,k}]^{-1/2} \frac{\partial \mathcal{C}_{1,k}}{\partial c_l} \right] \\ & - \frac{1}{6} \left[\frac{\mathcal{B}_{1,k}}{2} + \sqrt{\mathcal{C}_{1,k}} \right]^{-2/3} \left[\frac{\partial \mathcal{B}_{1,k}}{\partial c_l} + [\mathcal{C}_{1,k}]^{-1/2} \frac{\partial \mathcal{C}_{1,k}}{\partial c_l} \right], \end{aligned} \quad (20)$$

where

$$\begin{cases} \frac{\partial \mathcal{C}_{1,k}}{\partial c_l} = \frac{\epsilon_0}{\beta \Delta_z^k} \left[\left(\frac{\epsilon_0 J_z^{1,k}}{3\beta \Delta_z^k} \right)^2 (\varphi_z)_l^{1,k} - \frac{J_z^{1,k} \rho_{1,k-1}}{2} \frac{\partial \mathcal{B}_{1,k}}{\partial c_l} \right], \\ \frac{\partial \mathcal{B}_{1,k}}{\partial c_l} = -\frac{\epsilon_0}{\beta \Delta_z^k} \left(\rho_{1,k-1} (\varphi_z)_l^{1,k} + J_z^{1,k} \frac{\partial \rho_{1,k-1}}{\partial c_l} \right). \end{cases}$$

The derivatives are entirely determined by stating that $\rho_{1,1} = \rho_0$ is independent of c_l, and thus, $\frac{\partial \rho_{1,1}}{\partial c_l} = 0$.

The validation of the previous derivation, i.e., Eqs. (19) and (20), has been performed by comparison with approximate derivatives computed by divided finite differences.

4.2. *Examples*

We present now some numerical examples to evaluate the accuracy of the initial field reconstructed as described previously. The effect of the new initialization on the efficiency of the numerical computation of the electric field is also analyzed.

As a first example, configuration $\mathcal{A}$ is again considered here. Figures 9a and 9b, in which the plots corresponding to Figs. 5a and 5b are reported, show the improvement obtained on J when the KL parameterization is used instead of only the analytical field $\tilde{J}$. Moreover, Fig. 7 shows that now the relative error seems to be uniformly distributed on the computational domain, with an average error of about 20% along the z direction. However, it is also apparent that the c_l coefficient values obtained by the algorithm defined by Eqs. (16)–(20) (taking $i_0 = 3n_i/4$) are still rather far from optimal values. A first source of inaccuracy is due to the

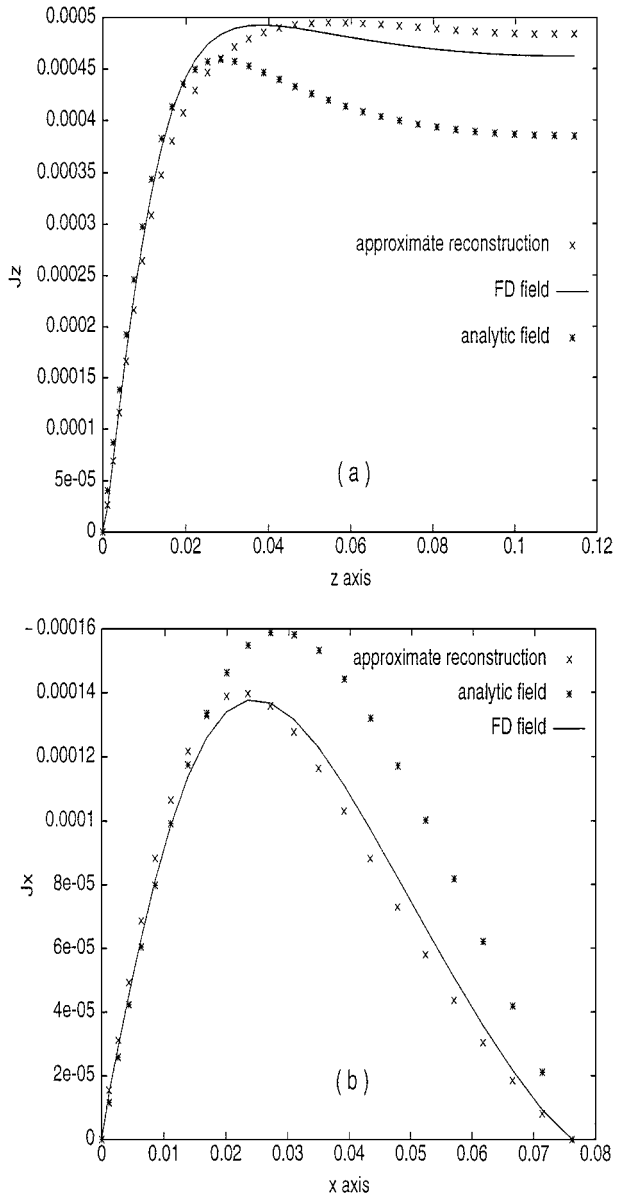

FIG. 9. Comparison of current density fields ($V_0 = 25.415$ kV and $a = 0.152$ mm): reference J, analytic approximation $\tilde{J}$, and approximate reconstructed field J^R, with $n_s = 10$, $n_m = 6$, and $i_0 = 3n_i/4$. (a) z component at $x = 0.0234$ m and (b) x component at $z = 0.0387$ m.

value of ρ_0 used in the algorithm, which is not the exact one but an estimate. But above all, the use of a Cartesian finite-difference method, which imposes a rectangular computational domain, does not allow the boundary conditions around the corona to be exactly imposed. Nevertheless, as shown in Fig. 8, in which the potential distribution along the line AB is plotted, a large improvement with respect to the analytical formula of Cooperman is also obtained for the potential field by using Eqs. (16)–(20). Apparently, in some cases the proposed reconstruction may be used directly to obtain an acceptable approximation of the exact solution at a negligible computational cost. Indeed, in the considered case,

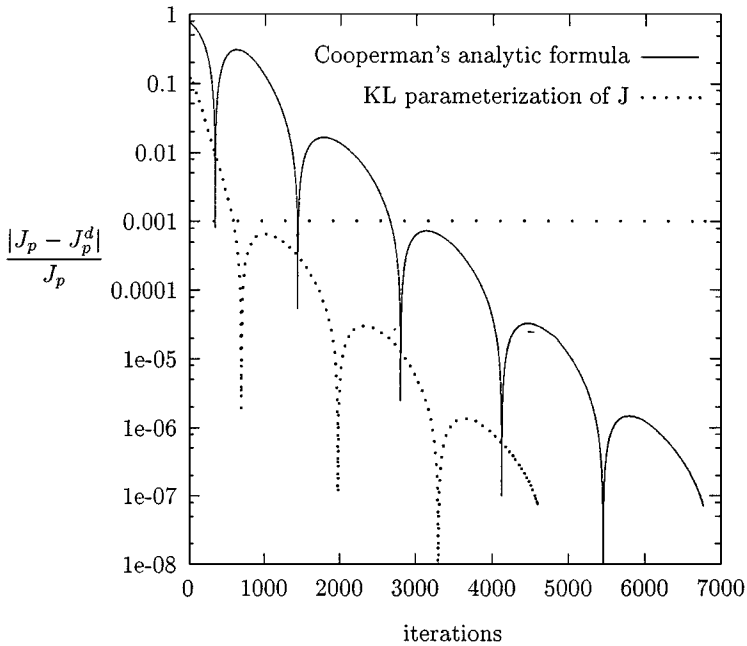

FIG. 10. Convergence histories for the configuration $a = 0.152$ mm and $V_0 = 25.415$ kV. Initial fields: Cooperman's analytic solution and the solution obtained using a KL parameterization for J with $n_s = 10$, $n_m = 6$, and $i_0 = 3n_i/4$.

approximately 0.1 s CPU is required on a PC to compute this approximation, while the numerical solution of the reduced Maxwell equations by the previously described finite-difference solver takes about 1 h CPU. The reconstructed field can also be used, as mentioned previously, as initialization for standard numerical solvers of the original Maxwell problem. The effect of more suitable initial V and ρ fields is clearly shown in Fig. 10, in which the convergence histories for both our approach and the classical initialization are shown. In particular, the logarithm of $|J_p - J_p^d(k)|/J_p$ is shown as a function of the iteration number. The form of the convergence curve is due to the fact that the term $(J_p - J_p^d(k))$ does not decrease uniformly to zero, but oscillates with values which can be both positive and negative. Thus, the local minima are due to the change of sign in $(J_p - J_p^d(k))$ values. In practice, convergence is considered reached only if Eq. (6) is verified for l consecutive iterations (we take here $l = 40$) to avoid local minima. A very fast initial convergence rate is observed with the new approach, which allows one to reduce the number of iterations by about 80% (566 instead of 2654) to reach an agreement between computed and specified values of J_p within 0.1%. The gain in efficiency obtained by this faster convergence is not decreased by the cost of the computation of the initial V and ρ fields. Indeed, the cost of the whole initialization procedure presented in Section 4.1 has been found to be lower than that of the classical initialization, in which the truncated Cooperman series [14] is used at each mesh point.

In Figs. 11 and 12 the convergence history for two other cases is shown. In the case of Fig. 11, which corresponds to the configuration $V_0 = 55$ kV and $a = 0.85$ mm ($J_p \simeq 1.33 \times 10^{-3}$ A/m^2), i_0 is taken equal to $3n_i/4$ for the potential field construction. The convergence improvement here is more limited, with a reduction of about 40% in the number of iterations (1507 instead of 2609). Conversely, very good convergence behavior is observed for the case

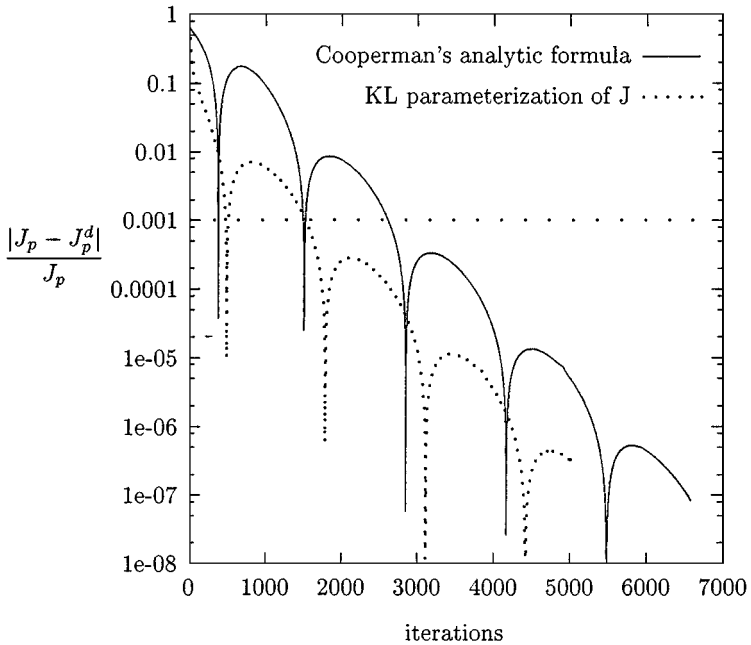

FIG. 11. Convergence histories for the configuration $a = 0.85$ mm and $V_0 = 55$ kV. Initial fields: Cooperman's analytic solution and the solution obtained using a KL parameterization for J with $n_s = 10$, $n_m = 6$, and $i_0 = 3n_i/4$.

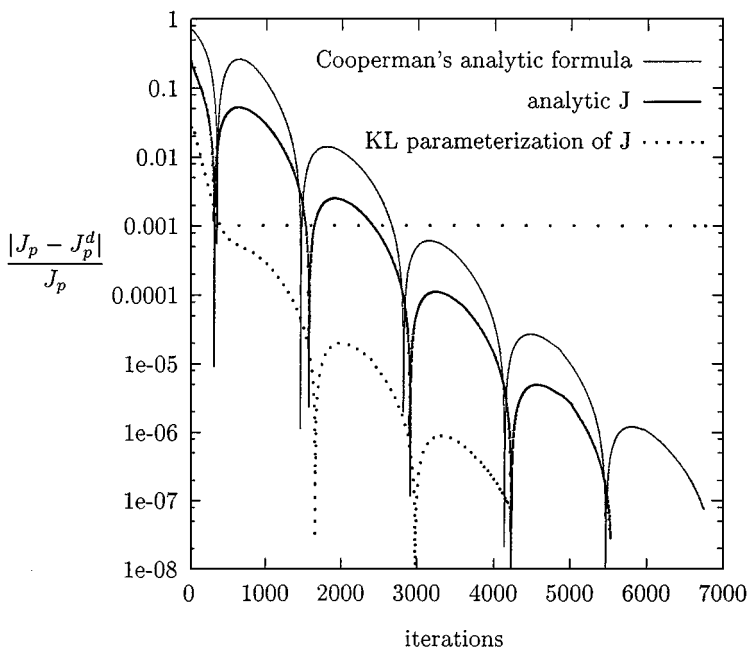

FIG. 12. Convergence histories for the configuration $a = 0.3$ mm and $V_0 = 35$ kV. Initial fields: Cooperman's analytic solution, the solution obtained using $\tilde{J}$, and the solution computed using a KL parameterization for J with $n_s = 10$, $n_m = 6$, and $i_0 = n_i/2$.

shown in Fig. 12, with more than 85% reduction in the number of iterations (385 instead of 2652). A gain of only 10% is achieved by using the analytical field $\tilde{J}$ for the initialization. This case corresponds to the configuration $V_0 = 35$ kV and $a = 0.3$ mm ($J_p \simeq 5.94 \times 10^{-4}$ A/m^2) and $i_0 = n_i/2$. This particularly fast rate of convergence coincides with a very good agreement of the initial potential field, as shown in Figs. 13a and 13b.

The performance of the present algorithm depends on both the particular considered case and the way the potential field is constructed, i.e., on the choice of i_0. For this precipitator

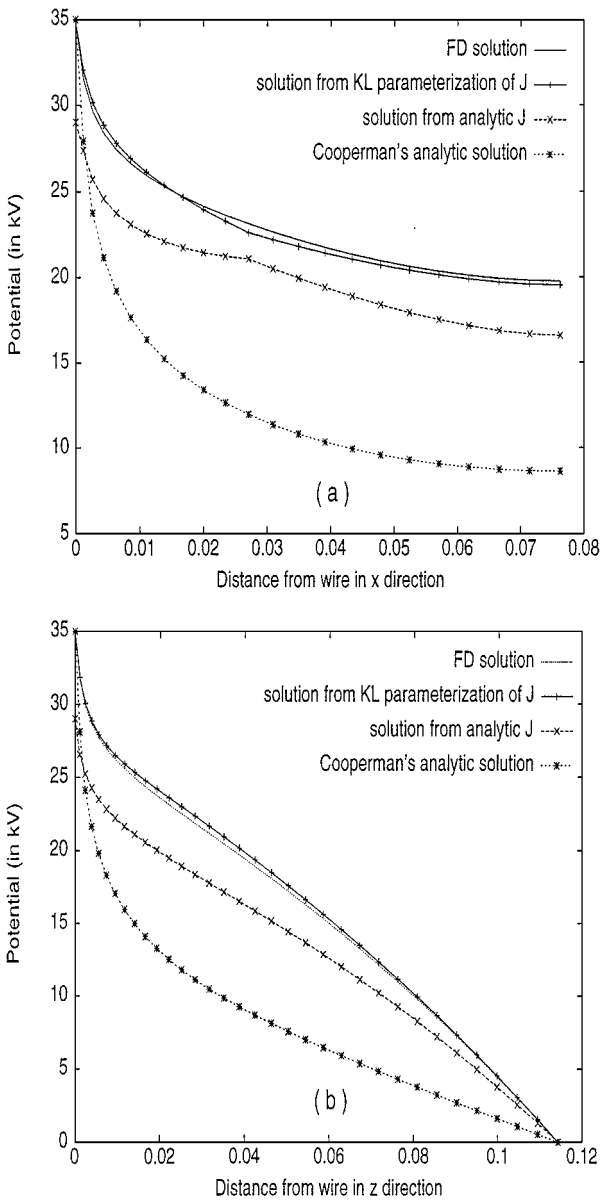

FIG. 13. Electric potential fields ($a = 0.3$ mm and $V_0 = 35$ kV) for the fully converged solution, Cooperman's analytic solution, the solution from $\tilde{J}$, and the solution from J^R with $n_s = 10$, $n_m = 6$, and $i_0 = n_i/2$. Potential (a) along AB and (b) along AD.

geometry, the best results are obtained for i_0 between $n_i/2$ and $3n_i/4$, i.e., taking x_{i_0} between $h_x/3$ and $2h_x/3$. However, the efficiency of the numerical computation was significantly increased by the new initialization in all the cases and for all the choices of i_0 that were tested.

The initialization of the ρ and V fields is strictly related to the numerical method used to discretize the problem. We have used here a finite-difference approach similar to the one employed in the numerical solution of the reduced Maxwell equations described in Section 2. Nevertheless, the analytical field $\tilde{J}$ and also the KL decomposition are independent of the particular discretization, and thus, starting from Eq. (15) other approaches can be developed to obtain the ρ and V fields. It is likely that the use of a more suitable discretization method, in which the corona boundary conditions are well imposed, might improve substantially the optimization algorithm, even though in this case, the explicit extraction of an exact gradient as done in Eqs. (19) and (20) could be more critical. Nevertheless, thanks to the low cost of the algorithm, an approximate gradient computation by divided finite differences can be envisaged without particular drawbacks.

Obviously, the efficiency improvement of the numerical solution of the original electrostatic problem obtained with the new initialization procedure may quantitatively depend on the particular solver used. Thus, present results can only give a qualitative indication. However, it is reasonable to infer that a more accurate initialization should lead to a substantial reduction of the computational cost for all numerical solvers.

5. RECONSTRUCTION FROM A CURRENT DENSITY FIELD

For an optimal flow configuration in a wire–plate ESP [3, 5], the optimization procedure gives a value of J from which the operative electrostatic variables must be derived. In this section, we will show how this can be done.

From Eq. (15) and a given J, the charge density field can be easily obtained if ρ_0 is known. However, since in this case V_0 and a are unknown, it is not straightforward to find a wire-charge density value. An estimate of ρ_0 can be obtained in the following way. By assuming a linear variation of J close to the corona region in both x and z directions and by interpolating the J values near the wire, the corona current density J_0 is found as a linear function of the wire radius a. Then, using the approximation $J_0 = 2J_p h_x/\pi a$, a second-order equation in a is obtained. From the value of a and using Eqs. (3)–(5), both ρ_0 and V_0 are estimated.

From the discretization (16) defined in Section 4, with the estimated ρ_0 value, a charge density field is obtained, while the construction of the potential field is carried out using only Eq. (17). Indeed, starting from a known current field, the errors on E_z described in Section 4 do not appear here. These two fields are then used as initialization for the solution of Eqs. (1) and (2). The electrostatic governing equations are solved iterating on ρ_0 as described in Section 2, but here at each iteration V_0 is updated from ρ_0 and J_p. More precisely, for given ρ_0 and J_p, a second-order equation in $\sqrt{a}$ is obtained by combining Eqs. (4) and (5). Then, V_0 is given by the current–voltage formula, i.e., Eq. (3).

The distribution of the resulting potential field along AD is plotted in Fig. 14a for configuration $\mathcal{A}$. This shows that a rather good approximation of the FD field is obtained with a computation cost equivalent to a direct resolution of the electrostatic problem. However, in the algorithm for the resolution of Eqs. (1) and (2) the iterative criterion is based on J_p; thus, only little information from the known J has been used, and moreover, the wire potential value V_0 is estimated from ρ_0 by a semiempirical formula. In some cases, the reconstruction

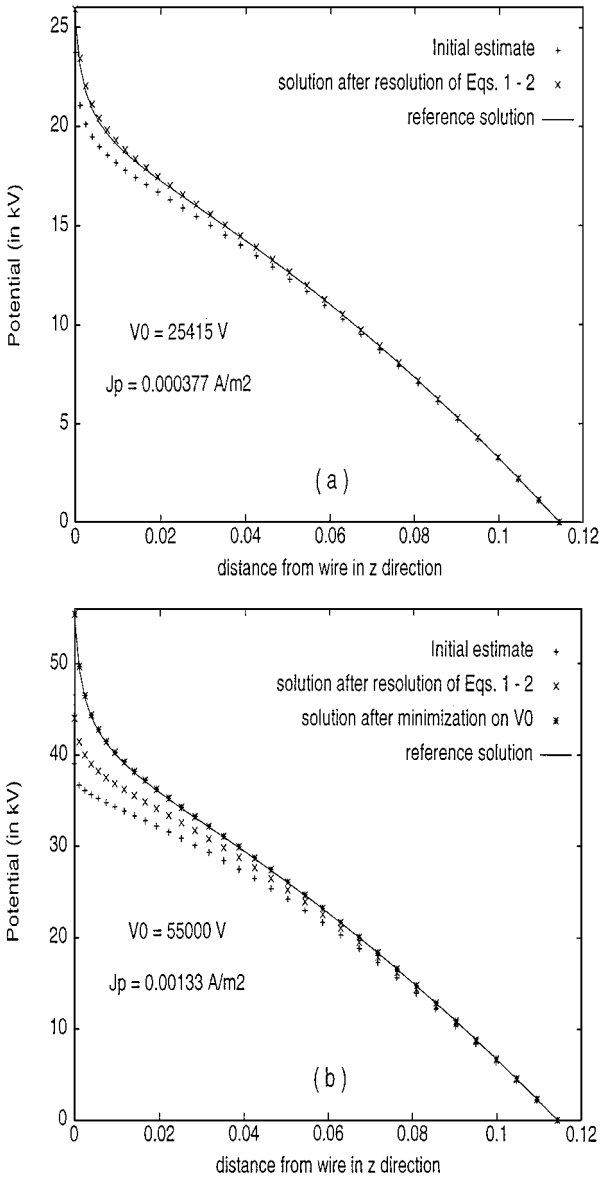

FIG. 14. Potential along AD for (a) configuration $\mathcal{A}$ and (b) $V_0 = 55\,\text{kV}$ and $J_p = 1.33 \times 10^{-3}\ \text{A/m}^2$. Comparison between the reference solution and the solutions after the different steps of the reconstruction.

procedure can give less accurate results, as shown in Fig. 14b, in which the potential distribution is plotted for the configuration defined by $V_0 = 55\,\text{kV}$ and $J_p = 1.33 \times 10^{-3}\ \text{A/m}^2$. To further improve the algorithm, an optimization can be done on the value of V_0 to obtain a current density field close to the desired one. With this aim, the following functional is defined,

$$\mathcal{I}(\bar{V_0}) = \frac{1}{(J_p)^2} \sum_{i,k} \| \bar{J}_{i,k} - J_{i,k} \|^2_{IR^2}, \tag{21}$$

where $\bar{J}$ represents the current density field obtained by solving the electrostatic governing

equations, (1) and (2), with the initial ρ and V fields from Eqs. (16) and (17), and $\bar{V_0}$ as wire-potential value. The corresponding wire radius $\bar{a}$, which is useful to define an initial ρ_0 value, is obtained from Eq. (3) by a Newton algorithm.

A classical univariate minimization is applied on $\mathcal{I}(V_0)$ with an initial search of the interval in which the minimum is located, completed by a quadratic interpolation algorithm.

Starting from the values obtained by the initial reconstruction algorithm, which gives in this case $\tilde{V}_0 = 43.79$ kV and $\mathcal{I}(\tilde{V}_0) = 27.69$ (see also Fig. 14b), after 15 cost function evaluations a large reduction of the functional $\mathcal{I}$ is obtained with $V_0^* = 55.196$ kV and $\mathcal{I}(V_0^*) = 5.07 \times 10^{-4}$. Because of better convergence in the solution of Eqs. (1) and (2), the CPU cost of this minimization is only about four times the cost of the initial reconstruction. The good behavior of the reconstruction is shown in Fig. 14b, in which the reconstructed potential is plotted after 11 cost evaluations ($\mathcal{I} = 3.29 \times 10^{-3}$).

The complete procedure, including the minimization of $\mathcal{I}(V_0)$, is more suitable for practical applications, in which the solution to be reconstructed is obviously not known. In this case, the accuracy of the reconstructed field can be measured by the reduction of the functional value.

6. CONCLUSIONS

The numerical computation of the ionic space charge and of the electric field produced by corona discharge in an electrostatic precipitator has been considered.

An analytical approximation of the current density field has been obtained, which is divergence free and satisfies the same boundary conditions as the exact field. This analytical approximation is derived under the additional assumption of irrotationality of the current density field and is obtained by singularity distributions and elliptic functions, classical tools used for hydrodynamic problems.

Since the approximated current density field satisfies the exact boundary conditions of the problem, a homogeneous field can be obtained, which can be parameterized by the Karhunen–Loève decomposition. The current density field is thus expressed as the sum of its analytical approximation and a linear combination of the KL functions. We compared the current density field obtained from a reference numerical solver to those recovered from the KL decomposition, with only a limited number of modes, for different configurations. The reference solution was given by a standard finite-difference solver of the partial difference equations governing the original problem, the accuracy of which was assessed by comparison with experimental data and by grid independence analysis. It has been shown that only very few KL modes, typically three or four, are needed to obtain an accurate reproduction of the reference field. Thus, the proposed parameterization could be useful in many practical applications, for instance, when the current density field must be optimized to a certain target (turbulent drag reduction, particle deposition increase). Note that the volume force experienced by charged particles or by the fluid in an electrostatic precipitator depends only on the current density field.

Moreover, the analytical approximation of the current density field can be used to obtain a guess of the ionic space charge and of the electric field. Starting from the knowledge of the current density field and from an empirical estimate of the wire-charge density value, the ionic space charge and the electric field can be reconstructed numerically. The same procedure can be used starting from the KL decomposition of J, in which the unknown coefficients are estimated by an optimization algorithm to obtain a global electric field which

gives the exact value of the potential at the wire (input of the problem). It has been shown that the resulting reconstruction of the global electric field is very close to the exact one, and in many cases it could be considered a satisfactory approximation of the exact solution, obtained at a negligible computational cost. In all cases, it is significantly more accurate than the initial guesses based on empirical formulas, which are typically used to initialize all numerical solvers. Consequently, by employing the proposed reconstruction for the initialization, the efficiency of the iterative numerical solver of the original problem increases significantly (up to a factor of 85%) and, hence, the computational cost is substantially decreased. Even though we obtained these results for a particular solver of the reduced Maxwell equations, it seems reasonable to extend the validity of our findings to any other iterative solver, at least from a qualitative viewpoint.

Finally, a procedure has been proposed to reconstruct the solution of the original Maxwell problem from a given current density field. This is of significance in practical applications to obtain, for instance, the electric configuration that gives a calculated optimized current density field. In this case, however, the values of both space charge and potential at the wire are unknown. An empirical estimate is used as initial guess and the electric and space-charge fields are reconstructed following the procedure described previously. Then, they are employed to initialize the numerical algorithm used for the solution of the original problem. In this procedure, the value of the space charge at the wire is progressively updated and the convergence criterion is based on the value of the current density at the plate, which is known. Simultaneously, an optimization algorithm, in which the wire potential is also progressively updated, is carried out to ensure that the global electrostatic solution obtained from the proposed procedure corresponds to a current density field as close as possible to the given one. The accuracy of the reconstruction has been assessed by comparison with reference direct solutions of the original Maxwell problem for different configurations. The computational cost is significant, but this reconstruction must be carried out only once, when the optimum J field has been obtained.

ACKNOWLEDGMENTS

Professor Luca Zannetti is gratefully acknowledged for valuable recommendations concerning elliptic functions. Special thanks go to Professor Guido Buresti for several useful remarks.

REFERENCES

1. G. Kallio and D. Stock, Interaction of electrostatic and fluid dynamic fields in wire–plate electrostatic precipitators, *J. Fluid Mech.* **240**, 133 (1992).
2. A. Soldati, On the effects of electrohydrodynamic flows and turbulence on aerosol transport and collection in wire–plate electrostatic precipitators, *J. Aerosol Sci.* **30**, 293 (2000).
3. A. Soldati and S. Banerjee, Turbulence modification by large-scale organized electrohydrodynamic flows, *Phys. Fluids* **10**, 1742 (1998).
4. W. Schoppa and F. Hussain, A large-scale control strategy for drag reduction in turbulent boundary layers, *Phys. Fluids* **10**, 1049 (1998).
5. M. Fulgosi, S. Banerjee, and A. Soldati, *Turbulence Modulation by an Array of Large-Scale Streamwise Structures of EHD Origin*, ASME Paper FEDSM99-6934 (1999).
6. J. R. McDonald, W. B. Smith, and H. W. Spencer III, A mathematical model for calculating electrical conditions in wire–duct electrostatic precipitation devices, *J. Appl. Phys.* **48**(6), 2231 (1977).

7. G. Kallio and D. Stock, Computation of electrical conditions inside wire–duct electrostatic precipitators using a combined finite-element, finite-difference technique, *J. Appl. Phys.* **59**(6), 1799 (1986).
8. E. Lami, F. Mattachini, R. Sala, and H. Vigl, A mathematical model of electrostatic field in wires–plate electrostatic precipitators, *J. Electrostat.* **39**, 1 (1997).
9. T. Yamamoto and H. R. Velkoff, Electrohydrodynamics in an electrostatic precipitator, *J. Fluid Mech.* **108**, 1 (1981).
10. S. Cristina, G. Dinelli, and M. Feliziani, Numerical computation of corona space charge and V–I characteristic in dc electrostatic precipitators, *IEEE Trans. Ind. Appl.* **27**(1), 147 (1991).
11. A. J. Medlin, *Electrohydrodynamic Modelling of Fine Particle Collection in Electrostatic Precipitators*, Ph.D. thesis (University of New South Wales, Sydney, 1998).
12. P. L. Levin and J. F. Hoburg, Donor cell-finite element descriptions of wire-duct precipitator fields, charges, and efficiencies, *IEEE Trans. Ind. Appl.* **26**(4), 662 (1990).
13. J. Q. Feng, Application of Galerkin finite-element method with Newton iterations in computing steady-state solutions of unipolar charge currents in corona devices, *J. Comput. Phys.* **151**, 969 (1999).
14. P. Cooperman, Research Cottrell Inc., Bound Brook, NJ, Report 46 (1952).
15. M. Loève, *Probability Theory* (Van Nostrand, Princeton, NJ, 1955).
16. G. Cooperman, A new current–voltage relation for duct precipitators valid for low and high current densities, *IEEE Trans. Ind. Appl.* **IA-19**(2), 236 (1981).
17. P. Cooperman, A theory for space-charge-limited currents with application to electrical precipitation, *AIEE Trans.* **79**, 47 (1960).
18. F. W. Peek Jr, *Dielectric Phenomena in High Voltage Engineering* (McGraw-Hill, New York, 1924), p. 66.
19. A. J. Butler, Z. J. Cendes, and J. F. Hoburg, Interfacing the finite-element method with the method of characteristics in self-consistent electrostatic field models, *IEEE Trans. Ind. Appl.* **25**(3), 533 (1989).
20. M. Abdel-Salam and Z. Al-Hamouz, Finite-element analysis of monopolar ionized fields including ion diffusion, *J. Phys. D: Appl. Phys.* **26**, 2202 (1993).
21. G. W. Penney and R. E. Matick, *Trans. Am. Inst. Electr. Eng.* **79**, 91 (1960).
22. F. Tricomi, *Funzioni Ellittiche* (Zanichelli, Bologna, 1951).
23. G. Berkooz, P. Holmes, and J. L. Lumley, The proper orthogonal decomposition in the analysis of turbulent flows, *Ann. Rev. Fluid Mech.* **25**, 539 (1993).